EUROPEAN ORGANIZATION FOR NUCLEAR RESEARCH
CERN - PS DIVISION

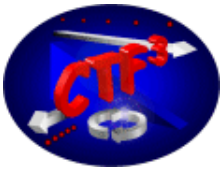

CTF3 Note 037
PS/AE Note 2001-016
(Preliminary Phase)

CTF3 Preliminary Phase Commissioning Report on Second Week, 8-12 October 2001

R. Corsini, B. Dupuy, L. Rinolfi, P. Royer (Ed.), F. Tecker, CERN, Geneva
O. Coiro, F. Marcellini, A. Stella, INFN - LNF, Frascati

Abstract

In this note, we describe the beam studies done during the second week of commissioning of the Preliminary Phase of CTF3, from October 8^{th} to October 12^{th} 2001. The beam was transported up to the end of the linac, where the instrumentation section is located, and in the dump line HIP. After the spectrometer line was commissioned, the bunching system was optimised and beam energy measurements took place. The Cherenkov monitors located at the end of the linac were also tested and first streak camera images of the pulse were taken. Bunch length measurements, beam current calibration and magnet polarity checks also took place during the week.

Geneva, Switzerland
December 10, 2001

1 Goals

During this second week, the beam was transported up to the end of the linac and into the dump line HIP. The goal was the commissioning of the instrumentation sections located at the end of the linac (sections 36 and 37). We used the main diagnostics tools available in these sections: the SEM-Grid WL.MSH36 in the spectrometer line (using the bending magnet WL.BHZ36), the Transition-Cherenkov monitor WL.TCM37, the wire scanner WL.WBS37 and the available screens. After the bunching was optimised, energy measurements, optics measurements, streak camera measurements and magnet polarity checks were also performed.

2 Start-Up

A new procedure for the security patrol to be performed before closing the machine was issued and accepted by the PS security board. It takes into account the new layout of the machine in the buildings. The PS security board is working on a new version for next year.

On Monday, hardware tests of the power supplies began for the magnets in the linac and in the dump line. At the end of the day, most of the power supplies were in operation, except WL.QNF371. The current MIN/MAX values were updated in the control database according to the power equipment limits. In the same time, vacuum interlocks and security chain were also tested.

When switching on the gun at the end of the first day, a parasitic pulse was observed after the first pulse in single pulse operation. The problem was studied and solved by R.Pittin and H.Hellgren (see Gun log-book for details). We also observed that after having lowered the high voltage of the gun, and putting ”Off pulsing”, a small pulse remains. This is normal since the cathode is still pulsed at low voltage (around 400 V) and very few electrons are emitted. According to the gun specialists, there is no radiation hazard related to this phenomenon.

At the end of the first day, TIS checked the radiation levels in the klystron gallery, while the three modulators were operated close to their nominal powers (5 MW for MDK25 and 30 MW for MDK27 and MDK31). Close to klystron MDK31 the radiation reached 60 $\mu Sv/h$, and 30 $\mu Sv/h$ in the gallery around. TIS did not allow to run with such radiation levels in that zone, and some additional shielding needed to be installed on Tuesday in order to operate at nominal power in MDK31.

On Tuesday afternoon, the beam was transported at low current up to the section 37 at the end of the linac. However, beam stopper WL.STP37 was stuck closed because the interlock condition on the current of HIE.MSH33 was not correct (since the element was not powered this week). The interlock was short-circuited during the rest of the week in order to be able to open it and to send the beam in the dump line. The polarity in HI.BSH00 was reversed.

The slits WL.SLH27 and WL.SLV27 were tested and the values saved as reference in the working set correspond to the open position.

The RF timing was adjusted such that all the five pulses are accelerated with similar energies and energy spreads. For that purpose, the “Start klystron”, “Start RF” and “End RF” timings were modified. The reference values are summarised in Table 1. Operation with seven pulses was tested, but we were then close to the limits and new settings remain to be found in that case.

	MDK25	MDK27	MDK31
WX.SKLY	29908	29916	29912
WX.SRFP	29968	29976	29974
WX.ERFP	30055	30036	30033

Table 1: RF timing references for the three klystron-modulators for five pulse operation.

3 Spectrometer measurements

3.1 General remarks

The first spectra measurements were performed with a series of wires whose display was inverted with respect to their position in the SEM-Grid. This was fixed later in the week. The dispersion value which is used in the MSH software to compute the energy spread was wrong and the values of the energy spread read on the display were therefore wrong during all the week. In addition, also during the whole week, the calibration factors giving the integrated field as a function of the current in WL.BHZ36 were not precisely corresponding to the magnetic measurement data. The energy of the central wire read on the display was therefore overestimated. However, the values of the energy spread and of the energy of the central wire were corrected during off-line computations. Equation (1) gives the integrated field in WL.BHZ36 (in T.m) as a function of the current in the magnet (in A). Figure 1 shows the magnetic measurement points and the new calibration curve as a function of the current in WL.BHZ36. Figure 2 shows an example of energy spectrum after off-line correction of the calibration and of the value of the dispersion.

$$\begin{aligned} \int B\mathrm{d}l = & + 0.000110293 \\ & + 0.00409926 \times I \\ & - 0.000010472 \times I^2 \\ & + 0.000000627668 \times I^3 \\ & - 1.685690 \times 10^{-8} \times I^4 \\ & + 2.340920 \times 10^{-10} \times I^5 \\ & - 1.796350 \times 10^{-12} \times I^6 \\ & + 7.623960 \times 10^{-15} \times I^7 \\ & - 1.677910 \times 10^{-17} \times I^8 \\ & + 1.496500 \times 10^{-20} \times I^9 \end{aligned} \tag{1}$$

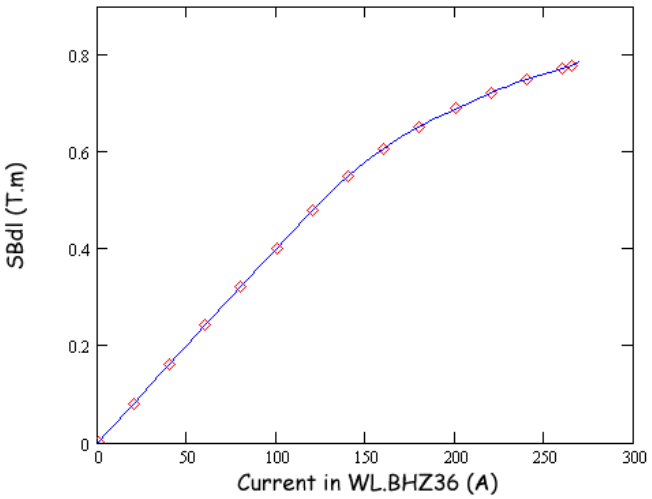

Figure 1: Magnetic measurements and calibration curve for the spectrometer magnet WL.BHZ36.

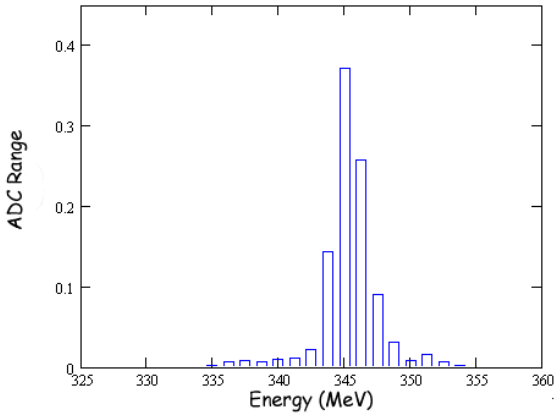

Figure 2: Energy spectrum recorded in the SEM-Grid WL.MSH36. In that case, the mean energy is 345 MeV and the rms energy spread is 2.29 MeV.

3.2 Total power versus beam energy

After having optimised the bunching system, some energy spectra were recorded for different powers in the modulators MDK27 and MDK31. The goal is to compare the beam energy read in the spectrometer and the beam energy computed from the values read in the peak power meters. The detailed formula to compute the energy gains from the values of the peak power meters is given in [1]. Figure 3 shows the plot of the beam energy as a function of the total power delivered by MDK27 and MDK31 (the energy at the end of the bunching system is assumed to be 5 MeV). In this plot the correct calibration factors of WL.BHZ36 are used to compute the energy measured in WL.MSH36. The error between the two curves is of the order of 3%.

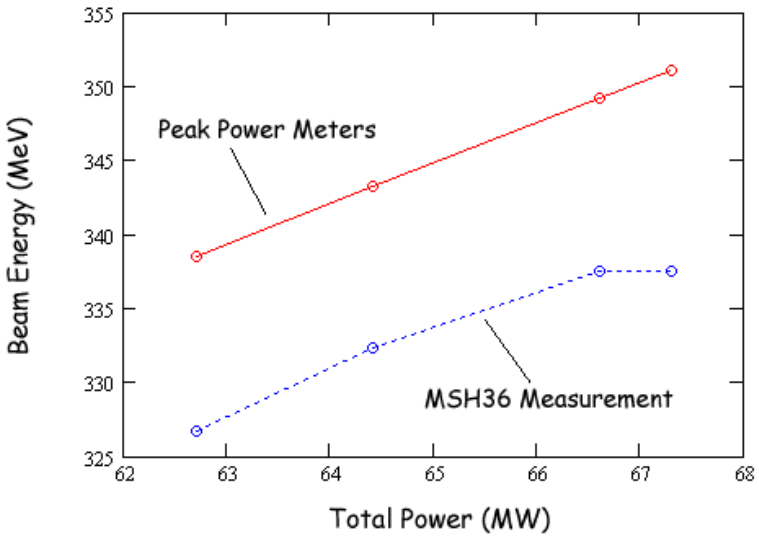

Figure 3: Beam energy as a function of the total power in modulators. Comparison between the energy measured in the spectrometer and the energy computed from the peak power meter values.

3.3 Bunch length measurement using phase method

We also took some energy spectra for different phases in MDK25, in order to measure the bunch length, as described in [2]. All the spectra were analysed using the new calibration factors for WL.BHZ36, and the correct value of dispersion was used off-line to compute the energy spread. Figure 4 shows the results obtained during this measurement. The data match the simulated energy spread for a Gaussian bunch of length 7 ps FWHM. The value of the uncorrelated energy spread is 1.95 MeV, which is comparable to the values we had during the same kind of measurements on the LPI machine [3]. Figure 4 also shows the curve for a bunch length of 20 ps FWHM, as measured during the Cherenkov monitor first tests (see Section 4): the measured energy spread is always far below this curve (even for a zero uncorrelated energy) and 20 ps FWHM is therefore an upper limit for the bunch length.

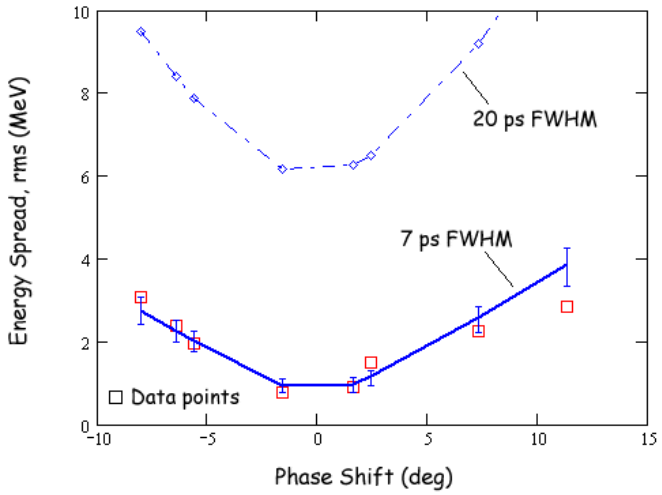

Figure 4: Bunch length measurement using phase of MDK25. The data points correspond to a 7 ± 1 ps FWHM bunch length. The uncorrelated energy spread is 1.95 MeV.

4 Transition-Cherenkov Monitors measurements

First tests of TCM took place during two days using the Cherenkov screen of WL.TCM37 in the matching section of the linac. At the beginning, in order to have visible light in the Streak Camera Lab, the repetition rate was increased from 50 Hz to 100 Hz and the current was increased to 200×10^8 electrons per pulse with 5 pulses. The light path was adjusted to the streak camera which was first used in focus mode because of timing problems. Later, in order to set-up the timing, a diode was used instead of the synchrotron light. This allowed to have timing references for the five sweep speeds of the streak camera. These timings were later refined using beam measurements. Table 2 sums up the reference values for the coarse timing (HX.SSTREAK-C) which counts the RF pulses, and for the fine delay (HX.SSTREAK) which counts in steps (one step is 0.205 ns). Figure 5 shows the image of one pulse recorded at the slowest sweep speed (1000 ps/mm). One can count 17 bunches inside this pulse, the intensity in WL.UMA36 at the end of the linac was 140×10^8 electrons per pulse.

Sweep speed	HX.SSTREAK-C	HX.SSTREAK
1000 ps/mm	30011	110-127
260 ps/mm	30012	24
150 ps/mm	30012	62
100 ps/mm	30012	62
50 ps/mm	30012	68

Table 2: References of the “Start Streak Camera” timing for the various sweep speeds.

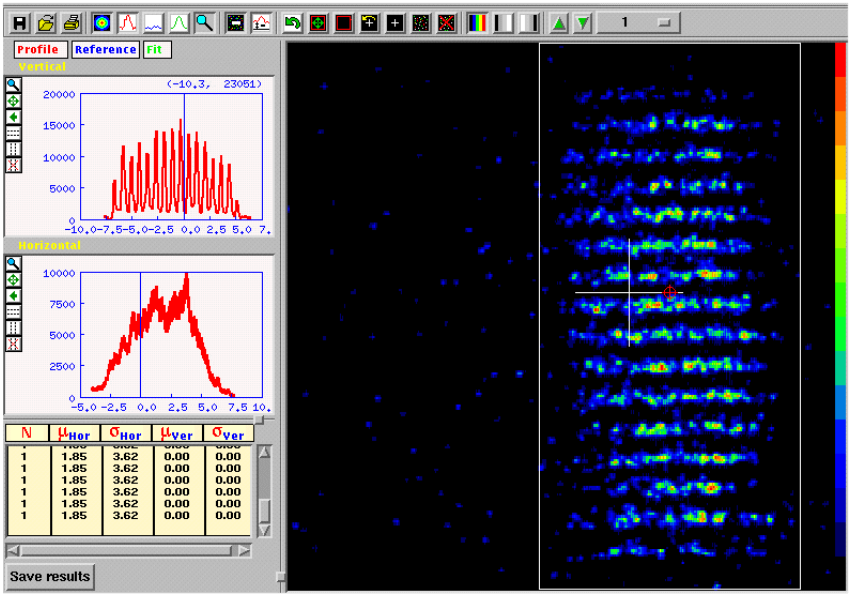

Figure 5: Streak camera image of the pulse from WL.TCM37 at the slowest sweep speed.

For each time scale of the streak camera, we recorded images of the pulse and of the bunches. It was then possible to calibrate the various speeds by measuring the bunch spacing, which is given by the 3 GHz RF frequency and is therefore 333 ps. For that purpose, we fit two consecutive bunches of the time profiles with Gaussian distributions. We checked that the sweep speed is constant over the range of the image by measuring the distance between different bunches of the same pulse. Table 3 gives the calibration factors for each sweep speed (except for 1000 ps/mm where the precision on the distance between bunches is not high enough on the profiles). These factors are used to convert the time scale from the software arbitrary units into picoseconds.

Sweep speed	Calibration factors
260 ps/mm	127.0
150 ps/mm	67.2
100 ps/mm	48.7
50 ps/mm	27.0

Table 3: Calibration of the sweep speeds of the streak camera using measurements done in WL.TCM37. These factors are used to convert the time scale from the software arbitrary units into picoseconds.

Knowing the calibration factors, we were able to have a first estimate of the bunch length by fitting the profiles with Gaussian distributions. A value of 20 ps FWHM was found for each sweep speed. Figure 6 shows the case of the 100 ps/mm sweep scale. However, this is much larger than the one obtained from the bunch length measurement using the phase shift method (7 ps FWHM, see Section 3.3). The reason is that many optical effects can affect this measurement by reducing the resolution (chromatic effects, spherical aberrations, bad focalization in the streak camera). Optimising the light transport should result in the observation of a shorter bunch length.

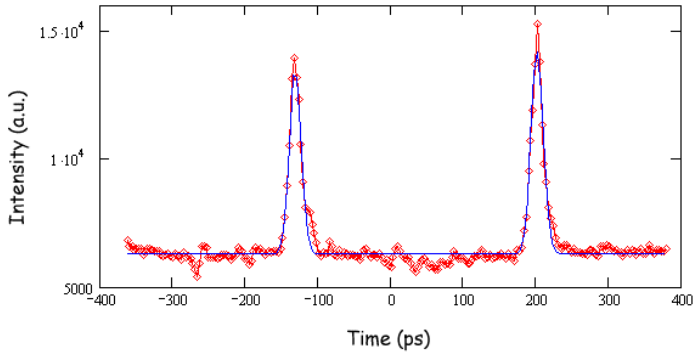

Figure 6: Streak camera profile and Gaussian fit for the sweep speed 100 ps/mm.

5 Beam Current Calibration

The calibration of the WL.ECM25 was cross-checked with the gun output and the first UMAs reading. The signals were observed from the rack behind HCR, knowing the gains of the various amplifiers located between the ECM and the signal output. The corresponding calibration factors to convert the amplitude of the signal into the beam current are available in the paper log-book. However, the amplitude of the signal is likely to be modified through the bandwidth of the amplifier. Therefore, the integral of the signal (which corresponds to the current) should be taken as the reference value. The ECM response was tested by P. Odier on a test bench. The software calibration factor was adjusted to cope with the response efficiency of the ECM. The gate to compute the integrated signal of the ECM was re-adjusted so that the integral stops at the zero crossing of the signal. The positive bump created by the electronics at the end of the signal (see Figure 7) is therefore not taken into account in the integral. High sensitivity on the limits of the integral was however observed.

Figure 7: ECM signal for the nominal current in the gun.

6 Magnet Polarity

During the polarity tests, the convention of using only positive currents in the power supplies was adopted. We then defined quadrupole and dipole types, according to the measured polarity in the machine. The different types as well as the specific actions taken are described in the paper log-book. During this tests, we noticed the following points:

- Almost no magnetic field was measured in the bucking coil solenoid because the supplied current was not sufficient (5 A instead of 100 A).
- No field was measured in the corrector WL.DQL29H on which the electrical connections were short-circuited. This was fixed.
- Corrector WL.DQNF37.2V had bad electrical connections. This was modified.
- Some quadrupole polarities were changed in order to use positive currents in all power supplies for the nominal optics (these quadrupoles are located in the matching section and in the transfer line, see paper log-book for details).
- Most of the dipoles in the linac had to be re-connected to agree with the conventions on the sign of the current and the resulting effect on the beam: for a positive current, deflection to the right for horizontal dipoles and upwards for vertical dipoles.

7 Various

- Quadrupole scans using WL.WBS31 were performed. The analysis will be presented together with the other quadrupole scans made during the following week of operation.
- Difference trajectories were also measured. Their analysis will be presented together with the quadrupole scans.
- WL.WBS28 and WL.WBS31 were checked. Signals looked correct but detailed tests are foreseen during next quadrupole scans.
- The WL.WBS37 data acquired by Excel showed a second peak which was not visible on the control software; This was due to a wrong size of the acquisition array in Excel and this had been fixed.

References

[1] R. Corsini, A. Ferrari, L. Rinolfi, T. Risselada, P. Royer, F. Tecker, “Beam Dynamics for the CTF3 Preliminary Phase”, CLIC Note 470.

[2] R. Corsini, A. Ferrari, L. Rinolfi, T. Risselada, P. Royer, F. Tecker, “LIL bunch length and lattice parameters measurements in March 2000”, PS/LP Note 2000-01 (MD), CTF3 Note 009.

[3] R. Corsini, A. Ferrari, L. Rinolfi, T. Risselada, P. Royer, F. Tecker, “New Measurements of the LIL bunch length and lattice parameters”, PS/LP Note 2000-02 (MD), CTF3 Note 013.